J. Mech. Phys. Solids 193 (2024) 105856

Contents lists available at ScienceDirect

Journal of the Mechanics and Physics of Solids

journal homepage: www.elsevier.com/locate/jmps

Cracking in semiconductor devices–effect of plasticity under triaxial constraint

Sammy Hassan [a], Jyun-Lin Wu [b], Jason Lan [b], Sherwin Tang [b], Jun He [b], Joost J. Vlassak [a], Zhigang Suo [a,*]

[a] *John A. Paulson School of Engineering and Applied Sciences, Kavli Institute for Bionano Science and Technology, Harvard University, MA, 02138, USA*

[b] *Quality and Reliability, Taiwan Semiconductor Manufacturing Company, Ltd., Hsinchu, Taiwan, Republic of China*

A R T I C L E I N F O

Keywords:
Semiconductor devices
Triaxial confinement
Plasticity
Cracking
Energy release rate

A B S T R A C T

A semiconductor device integrates dissimilar materials of small sizes and complex geometries. During fabrication, the materials are deposited at various temperatures. Both deposition and change in temperature cause stresses in the materials. Under the stresses, ductile materials may deform plastically, and brittle materials may crack. Here we focus on how plastic deformation in the ductile materials affects cracking in nearby brittle materials. We study a model structure in which a metal line is encased by a silicon substrate and a brittle oxide layer. In the triaxially constrained metal, the stresses readily exceed the yield strength of the metal. Such high stresses in the metal elevate the stresses in the oxide. The degree of triaxial constraint varies with the aspect ratio of the metal. We compute the stress in the oxide, as well as the energy release rate of an edge crack and a long channel crack. We discuss strategies to avert cracking in the oxide.

1. Introduction

In a semiconductor device, ductile and brittle materials are frequently used in close proximity. For example, a ductile metal, such as aluminum or copper, is used as an electrical conductor, and a brittle oxide, such as silica, is used as an electrical insulator. These materials are deposited on a silicon wafer. The metal typically has a larger coefficient of thermal expansion than the oxide and silicon. Consequently, the metal develops tensile stresses upon cooling from the processing temperature. The thermal mismatch also causes stresses in oxide and silicon. The stresses can plastically deform ductile materials (Cheng and Shen, 2012; Jawarani et al., 1997; Jiang et al., 2015) and crack brittle materials (Chen et al., 2022; Liu et al., 2000). The former and the latter are concurrent and affect each other.

A common configuration in a semiconductor device involves a metal line encased by an oxide and a silicon substrate (Fig. 1). Empirical observations indicate that the aspect ratio of the metal lines affects the likelihood of cracking in the oxide. Although a device in practice has a complex structure, here we focus on two features. First, assume that the aluminum is adherent to the oxide and silicon, so that the plastic deformation in the aluminum is constrained by the oxide and silicon. Second, a crack is found in the oxide layer near the aluminum line. Aluminum has a modest yield strength, and does not harden appreciably after yielding. Under uniaxial and biaxial stress, the aluminum does not develop stress much beyond the yield strength. Thus, it is often thought that the yield strength sets the

* Corresponding author.
E-mail address: suo@seas.harvard.edu (Z. Suo).

https://doi.org/10.1016/j.jmps.2024.105856
Received 12 June 2024; Received in revised form 22 August 2024; Accepted 7 September 2024
Available online 8 September 2024
0022-5096/© 2024 Elsevier Ltd. All rights are reserved, including those for text and data mining, AI training, and similar technologies.

stress level in aluminum in integrated structures, no matter how much the temperature drops. This expectation, however, is wrong when the oxide and silicon constrain the plastic deformation in aluminum in all three directions. Under the triaxial constraint, the aluminum develops triaxial tensile stresses, with magnitude often markedly exceeding the yield strength. The high triaxial stresses in aluminum is accompanied by high stresses in the surrounding materials. Whereas the oxide on top of the aluminum is under compression, the oxide between the two aluminum lines is under tension. The tension may crack the oxide, leading to electrical failure. Understanding the relationship between the constraint of the metal and the stresses in the oxide can help develop strategies to avert cracking in integrated structures.

Triaxial stresses in confined metal lines have been analyzed before. For example, high triaxial stresses in the metal can lead to void formation and growth (Flinn et al., 1993; Sullivan, 1996). Efforts have been made to understand the effect of the geometry of a constrained metal line on the triaxial stresses in the metal (Shen, 1997; Gouldstone et al., 1998; Park and Jeon, 2003; Ang et al., 2007; Shen, 2008). The effects of the properties of the materials encasing the metal, such as coefficients of thermal expansion and moduli, have also been studied (Sautera and Nix, 1990). However, little attention has been paid to the stresses in the surrounding materials. Here we study how the triaxial stresses in the metal affect the stresses and cracking in the surrounding materials.

2. A structure with a confined metal line

During the fabrication of a semiconductor device, dissimilar materials are deposited at different temperatures. Within each material, the deposition process induces stresses, called intrinsic stresses (Bromley et al., 1983; Lee et al., 1995). In addition, when the structure is cooled from the deposition temperature, dissimilar materials have different coefficients of thermal expansion, which also generates stresses, called thermal stresses. In this paper, to focus on main ideas, we will neglect intrinsic stresses and limit our attention to thermal stresses. Furthermore, to demonstrate salient features of triaxial constraint, we consider a simplified structure, in which an aluminum line is encased by a silicon oxide layer. Beneath the aluminum line is a thin layer of nitride and a silicon substrate (Fig. 2a).

Consider the magnitude of the stress of a blanket aluminum film on top of a silicon substrate upon cooling from a deposition temperature, T_i to a temperature T. If the aluminum is elastic, the film develops an equal biaxial stress of magnitude

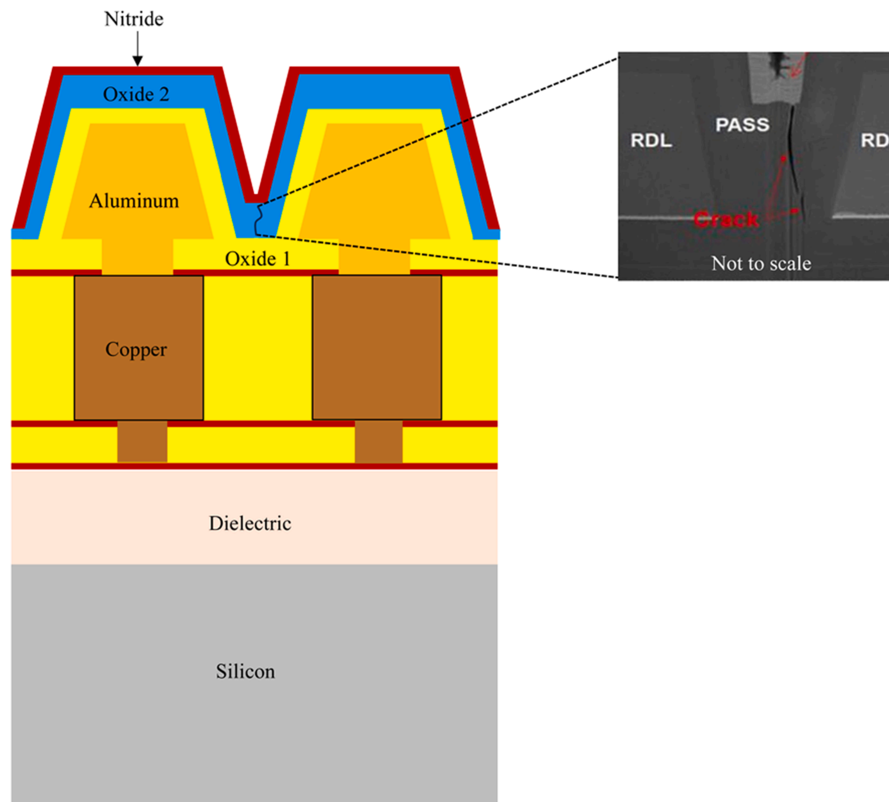

Fig. 1. Schematic of part of a semiconductor device. Dissimilar materials are integrated, including silicon, dielectric, nitride, oxide 1, oxide 2, copper, and aluminum. The integration of the dissimilar materials causes stresses. A crack is observed in oxide 2. The RDL refers to a redistribution layer and represents the aluminum line. The pass refers to a passivation layer and represents the oxide film. The crack is observed after a cool down from the deposition temperate to room temperature.

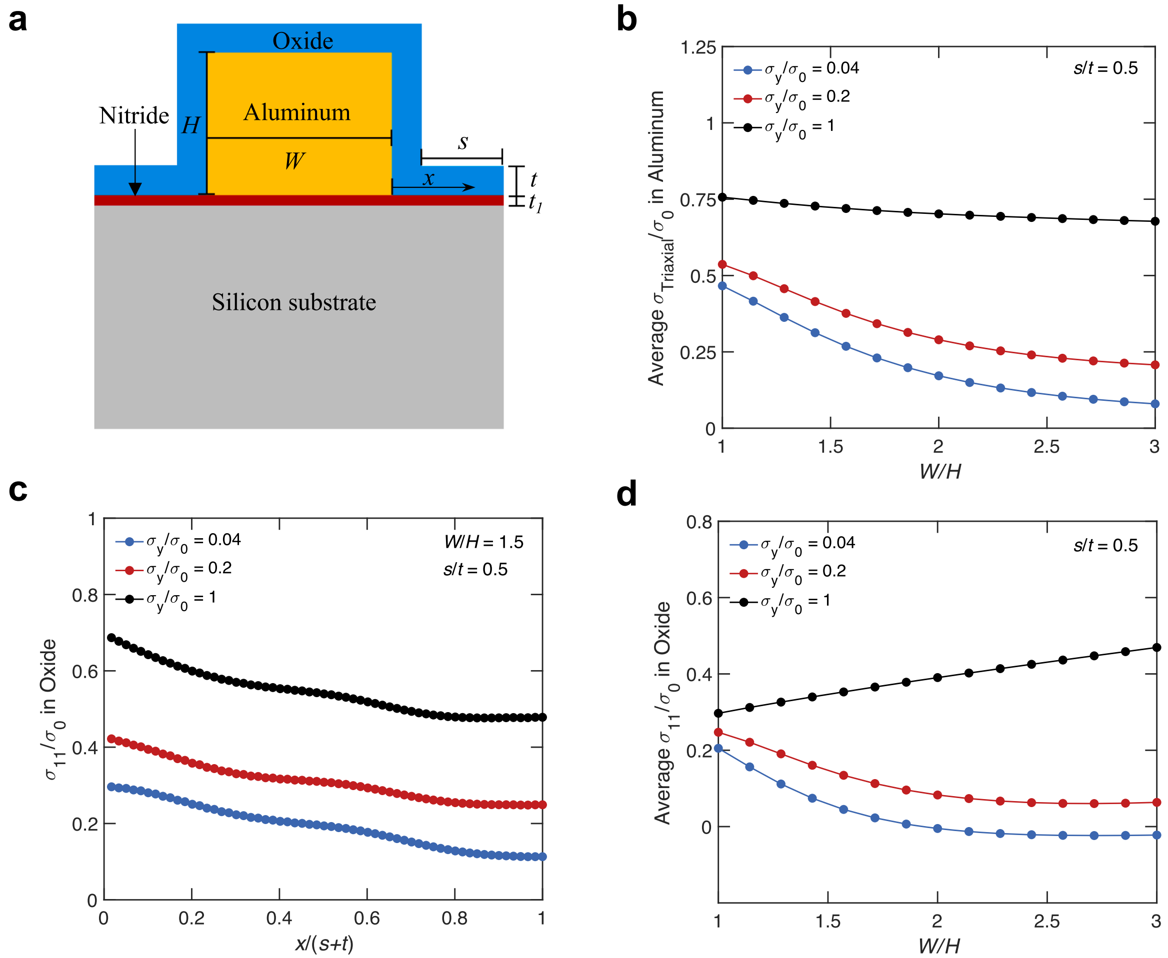

Fig. 2. Stresses in a simplified structure. (a) The structure consists of silicon, aluminum, oxide and nitride. (b) Average triaxial stresses in aluminum as a function of aluminum aspect ratio. (c) Transverse stress distribution in oxide as a function of position away from the aluminum. The stress is taken midway through the oxide thickness (d) Average transverse stress in oxide as a function of aluminum aspect ratio.

$$\sigma_0 = \frac{E}{1-\nu}(\alpha - \alpha_{Si})(T_i - T), \tag{1}$$

where α and α_{Si} are the coefficients of thermal expansion of aluminum and silicon, and E and ν are Young's modulus and Poisson's ratio of aluminum. Taking representative values, $E = 70$ GPa, $\alpha = 23 \times 10^{-6}$ °C^{-1}, $\alpha_{Si} = 3 \times 10^{-6}$ °C^{-1}, $\nu = 0.3$, $T_i = 500$ °C, and $T_f = 25$ °C (Sautera and Nix, 1990), we estimate that $\sigma_0 = 1.02$ GPa. In reality, aluminum undergoes plastic deformation. For simplicity, this paper models aluminum as an isotropic elastic-plastic material, and neglects strain hardening. Consequently, the biaxial stress in the aluminum film is limited by the yield strength of aluminum, which is on the order of 200 MPa.

Next, consider an aluminum line triaxially confined by the surrounding elastic materials. Under triaxial confinement, the stress in the aluminum can markedly exceed the yield strength. The magnitude of the triaxial stress in the metal depends on the aspect ratio, W/H. When the aspect ratio is small, the metal is triaxially confined, and plastic flow is restricted. When the aspect ratio is large, triaxial confinement is small, and plastic flow readily occurs. Note that the degree of triaxial confinement also depends on the ratio of the film thickness to metal thickness, t/H. When the thickness ratio between the film and the metal decreases, the amount of triaxial

Table 1
Material properties used for aluminum, oxide, silicon, and nitride.

Material	E (GPa)	v	α (10^{-6} °C^{-1})
Aluminum	70	0.35	23.6
Oxide	85	0.2	0.6
Silicon	110	0.28	3
Nitride	185	0.18	5

confinement is reduced (Sautera and Nix, 1990). In this paper, we vary the ratio W/H, but fix $t/H = 0.43$.

We model triaxial confinement using the commercial finite element software ABAQUS. Symmetric boundary conditions are imposed on both sides of the structure. The silicon substrate is an order of magnitude larger than the thickness of the aluminum and is assumed to be infinitely thick. We fix the vertical displacement on the bottom side of the substrate. Quadrilateral and triangular plane-strain elements are used throughout this paper. The mechanical properties are fixed in calculations (Table 1). All materials are modeled as linearly elastic, except aluminum, which is modeled as elastic-perfectly plastic. The nonlinear boundary value problem is solved by incrementally decreasing the temperature from the deposition temperature (500 °C) to room temperature (25 °C). The entire structure is assumed to be stress-free at 500 °C. The thickness ratio between the oxide and the nitride is set as $t/t_1 = 1.3$.

3. Stresses

We calculate the triaxial stress in the aluminum, σ_{Triaxial}, by taking the average of the three normal stresses. The volume-averaged triaxial stress in the aluminum is plotted as a function of aspect ratio for different values of the yield strength (Fig. 2b). Both the averaged triaxial stress σ_{Triaxial} and the yield strength σ_y are normalized by σ_0. When σ_y is comparable to σ_0, the aluminum line predominantly deforms elastically, and the triaxial stress decreases slightly with increasing aspect ratio. By contrast, when σ_y is less than σ_0, the aluminum line deforms plastically and the triaxial stress decreases appreciably with increasing aspect ratio. Plasticity makes the stress state in the line much more sensitive to its aspect ratio. A larger aspect ratio enables more plastic deformation in the metal, which can greatly relieve its stresses. Assuming $\sigma_y = 200$ MPa, $\sigma_{\text{triaxial}} = 560$ MPa when $W/H = 1$, but $\sigma_{\text{triaxial}} = 255$ MPa when $W/H = 3$.

We now study how the constrained plasticity in the aluminum affects the stress in the oxide. To highlight the effect of the triaxial constraint, we set the aspect ratio to $W/H = 1.5$. Fig. 2(c) plots the transverse tensile stress in the oxide σ_{11} as a function of normalized distance away from the aluminum for different values of the yield strength. The stress is taken midway through the oxide thickness. The tensile stress is highest near the interface with the aluminum and drops with distance away from the aluminum. The stress in the oxide is also a function of the yield strength of aluminum. The lower the yield strength, the lower the stress in the oxide. Plastic deformation in the aluminum reduces the magnitude of stress in the oxide.

Note that although the stress is highest near the aluminum, cracks are observed in practice at the location away from the interface, in the oxide at the midpoint between the two aluminum lines. This crack location may be due to the presence of defects during fabrication. We now examine the stress level in the oxide at the midpoint between the two aluminum lines. Fig. 2(d) plots the thickness-averaged tensile stress σ_{11} in the oxide as a function aspect ratio of the aluminum for different values of the yield strength. When σ_y is comparable to σ_0, the aluminum line predominantly deforms elastically, and stress in the oxide increases with the increasing aspect ratio. The wider the aluminum line, the higher the transverse stress in the line, and the higher the stress in the oxide. When σ_y is less than σ_0, the aluminum deforms plastically, and the stress in the oxide decreases with increasing aspect ratio of the aluminum. In the presence of plasticity, the increase in transverse stress associated with a wider pad is masked by the drastic reduction in stresses due to plastic deformation. Our results demonstrate that the degree of confinement of the metal line affects the stress level in the surrounding oxide film. In particular, increasing the aspect ratio of the metal line reduces the triaxial stresses within the aluminum,

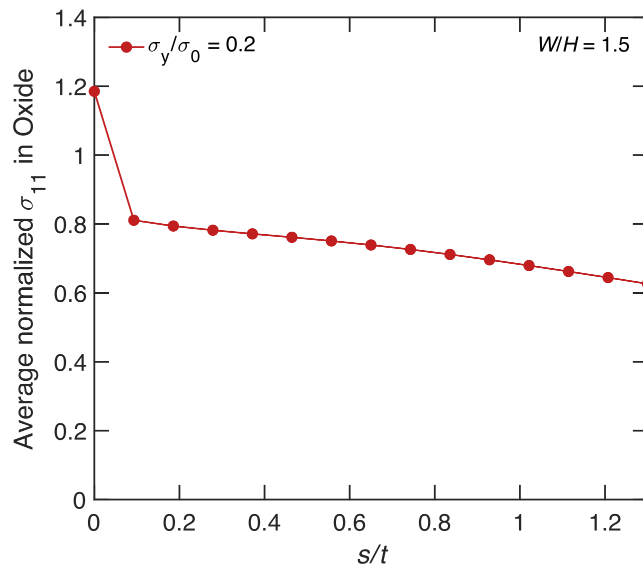

Fig. 3. Normalized transverse stress in oxide as a function of spacing between the aluminum lines. The stress is averaged along the thickness of the oxide and is taken at the midpoint between the two aluminum lines. The stress is normalized by the stress at the interface of the aluminum and the oxide.

4. Energy Release rate.

and thereby decreases the stress level in the oxide.

The oxide at the midpoint between the two aluminum lines is also susceptible to additional stresses incurred by the neighboring aluminum lines. To demonstrate the effect of a neighboring aluminum line, we perform a calculation using periodic boundary conditions on the left and right sides of the structure. We plot the transverse stress at the midpoint between the two aluminum lines and normalize it by the transverse stress at the interface of the aluminum line (Fig. 3). When $s = 0$, the stress at the midpoint exceeds that at the interface. This is due to the stress induced by the neighboring aluminum line. As the spacing increases, the stress at the midpoint between the two aluminum lines decreases but remains close to the stress at the interface. Consequently, cracks located in the oxide at the midpoint between the two aluminum lines can occur due to the overlapping stress fields caused by the aluminum lines.

To avoid cracking, two design approaches are commonly considered: one based on strength and the other based on toughness. In the strength-based approach, the strength of a material is experimentally determined. The stress field in the structure is then computed and the maximum stress is obtained. Provided the maximum stress does not exceed the strength, the structure is deemed safe. However, the strength-based approach is difficult to apply for two reasons. First, in a brittle material, such as silica, strength is not a material property. For instance, the theoretical strength of silica is high, but the experimental strength is reduced when the flaws exceed a few nanometers. Because the sizes of the flaws are random, the measured strength of silica has large statistical variation from sample to sample. Second, the stress field in a semiconductor device is highly sensitive to details of its geometry. Semiconductor devices frequently contain corners, where the stress field can also be singular.

By contrast, toughness is a material property. In the toughness-based approach, the toughness of a material is experimentally determined. One then calculates the energy release rate G of a pre-existing crack. The crack grows when the energy release rate exceeds the toughness. In this paper, we focus on the toughness-based approach.

In a semiconductor device, the location and size of a flaw are typically unknown. The application of the toughness-based approach requires pre-existing knowledge about the flaw, including its location, size, and orientation. For example, consider a crack of length c in the oxide layer. Dimensional analysis dictates that the elastic energy released per unit area of the crack should take the following form:

$$G = \frac{\sigma_0^2 t}{E} F\left(\frac{\sigma_y}{\sigma_0}, \frac{W}{H}, \frac{c}{t}, \frac{s}{t}, \frac{t_1}{t}\right) \tag{2}$$

where t is the thickness of the oxide and E is the modulus of the aluminum. Of all material properties, only the yield strength of the aluminum line will be varied here. Eq. (2) requires knowledge of the crack length and location. Cracks may grow in regions where processing defects are present or in areas of high stress concentration. These considerations can serve as guidelines for selecting a crack location. Once the crack location is set, one can calculate the energy release rate for various crack lengths and use the critical length for design. We first focus on a crack growing in a region where processing flaws are likely to be present, such as that shown in Fig. 1. A crack of length c is set in the oxide in between the two aluminum lines (Fig. 4a). We compute the energy release rate of the crack using the J-integral in ABAQUS. Fig. 4b plots the normalized energy release rate as a function of crack length for different values of the yield strength. The lower the yield strength of the metal, the smaller the energy release rate. This indicates that the plasticity in the aluminum reduces the energy release rate of the crack in the oxide. Note that for any value of the yield strength, the energy release rate increases with increasing crack length, peaks at an intermediate crack length, and drops to zero when $c/t = 1$. The drop in the energy release rate is due to the crack approaching the nitride interface, which has a larger modulus than the oxide. The flaw size corresponding to the peak energy release rate can be used as the critical flaw size for design. The critical flaw size varies somewhat with the aspect ratio of the metal line. For simplicity, we will assume the critical flaw size to be $c/t = 0.4$ when we study the effect of metal line

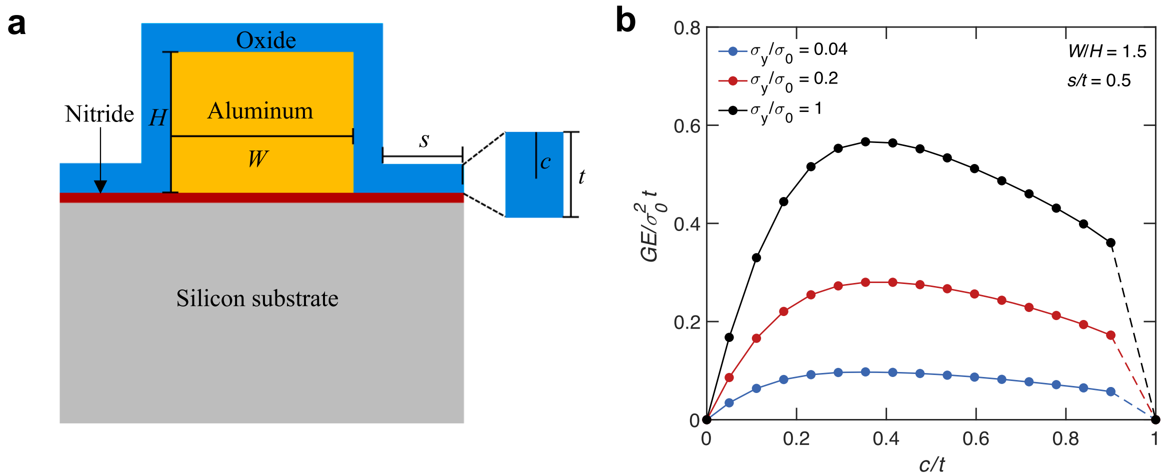

Fig. 4. Energy release rate of a crack in the middle of the oxide. Here we set $W/H = 1.5$ and $s/t = 0.5$. (a) A crack is introduced in the oxide (b) Energy release rate in oxide as a function of crack length for different values of the yield strength.

geometry on cracking in the oxide.

We next examine a crack located in the highest stress region. The analysis in Fig. 2c indicates that the transverse stress is highest near the interface of the aluminum line. In that region, oxide also forms a 90-degree corner with the aluminum and the underlying nitride. The stress concentration due to the corner can further increase the likelihood of crack initiation and growth. Consider a crack initiating at the oxide corner, located a distance $t/20$ away from the aluminum line interface (Fig. 5a). We plot the normalized energy release rate as a function of crack length for different values of the yield strength (Fig. 5b). When the crack length is small, $c/t < 0.5$, the energy release rate is lower for smaller values of the yield strength. However, for larger crack lengths, $c/t > 0.5$, smaller values of yield strength result in higher energy release rates. This difference in behavior occurs due to the competition between larger crack opening displacements and the reduced stresses associated with plastic deformation. Plasticity reduces the stresses in the oxide. However, because of the proximity of the crack to the interface, plasticity can greatly increase the crack opening displacement. To illustrate this effect, we plot contours of the crack opening displacements for a large crack, $c/t = 1$, for each of the yield strength values (Fig. 5c). A lower yield strength results in a larger crack opening displacement, which is associated with a greater amount of elastic energy released, and, consequently, a larger energy release rate. However, this effect is only pronounced when the crack length is large. For small crack lengths, $c/t < 0.5$, the energy release rate is dictated by the stress level in the oxide, which decreases with lower yield strength values. Note that, in principle, the crack length for such a crack can exceed $c/t = 1$. Since the oxide near the aluminum is under tensile stress, the crack would continue to grow vertically until it eventually reaches the compressive regions near the top surface of the oxide.

We now study the effect of geometry on the energy release rate of a crack in the oxide. First, we consider a crack in the oxide in between the two aluminum lines, as shown in Fig. 4(a). As noted before, we set the crack length to $c/t = 0.4$. Fig. 6(a) plots the normalized energy release rate versus aspect ratio for different values of the yield strength. When the yield strength is comparable to the thermal stress, the aluminum line deforms predominantly elastically, and the energy release rate increases with increasing aspect ratio. When the yield strength is less than the thermal stress, the line deforms plastically, and the energy release rate decreases with increasing aspect ratio of the aluminum. Next, we consider a crack near the interface of the aluminum line, as shown in Fig. 5(a). Recall that the energy release rate for such a crack monotonically increases with crack length. Therefore, we set the flaw size as $c/t = 1$, and plot the energy release rate as a function of aspect ratio of the metal line (Fig. 6b). When the aspect ratio is small, the energy release

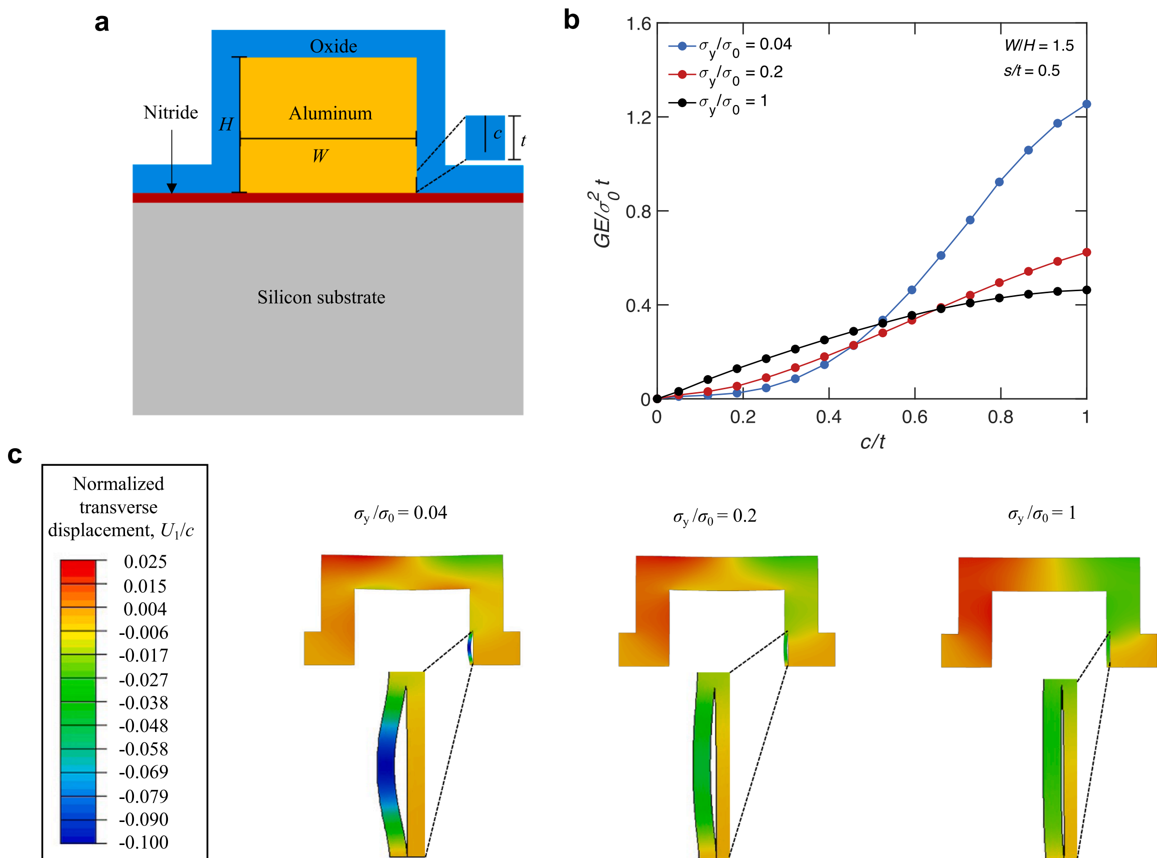

Fig. 5. Energy release rate of a crack in the corner of the oxide. (a) A crack is located in the oxide, at a distance $t/20$ away from the aluminum line (b) Energy release rate in oxide as a function of crack length. (c) Contour plots of the crack opening displacement for different yield strengths.

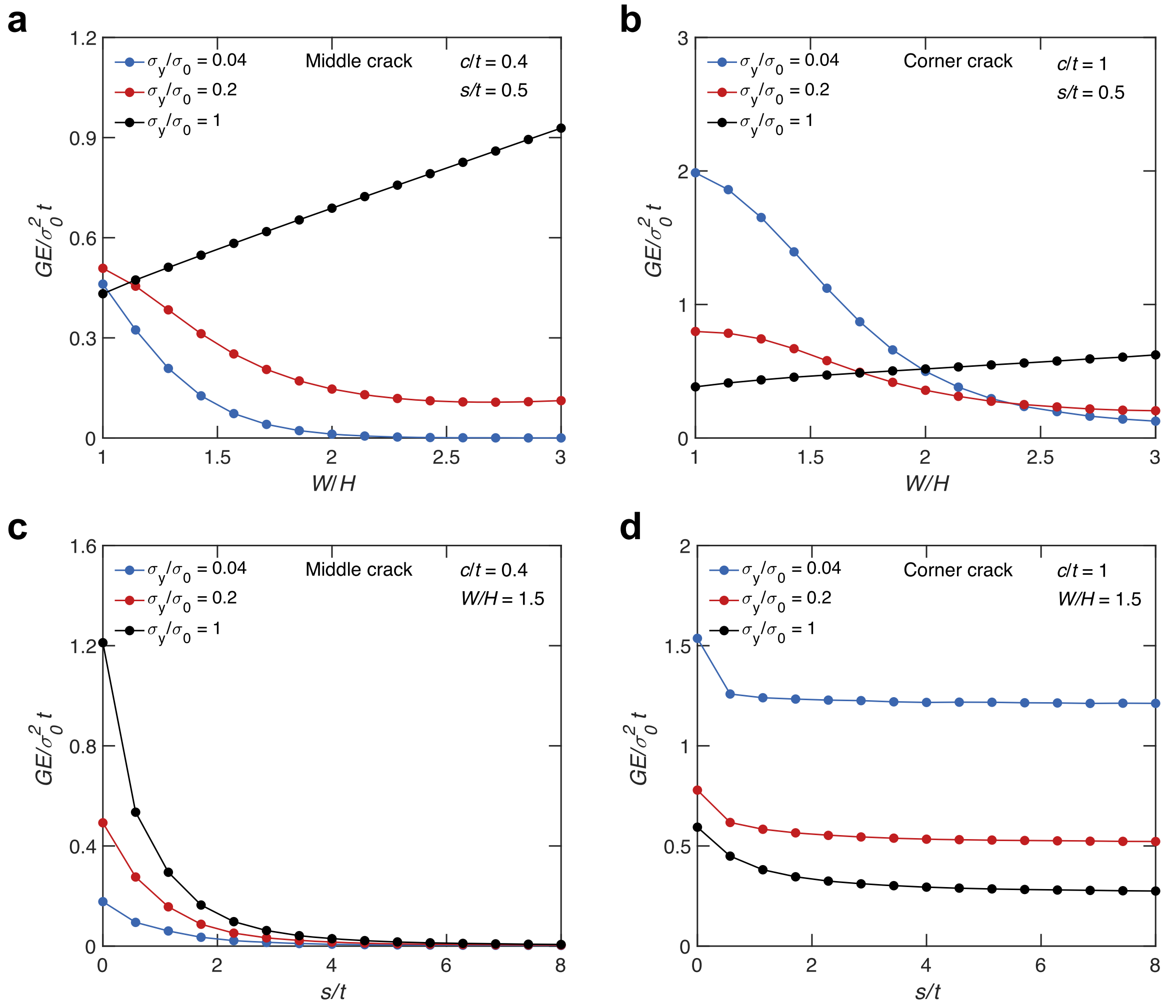

Fig. 6. Effects of geometry on energy release rate. (a) Energy release rate in oxide as a function of aspect ratio for a middle crack. (b) Energy release rate in oxide as a function of aspect ratio for a corner crack. (c) Energy release rate in oxide as a function of spacing for a middle crack. (d) Energy release rate in oxide as a function of spacing for a corner crack.

rate is higher for smaller values of the yield strength. This is due to the larger crack opening displacement associated with plastic deformation. However, for larger aspect ratios, smaller values of yield strength result in lower energy release rates. The reduction in energy release rate due to increased plastic flow masks the increase in energy release rate due to a larger crack opening crack displacement. We next study the effect of the line-to-line spacing. Fig. 6(c) plots the energy release rate as a function of spacing for a crack located in the middle of the oxide layer. Our results indicate the critical role that the geometry of the structure plays in driving the crack. Wide metal lines not only reduce the stress state in the metal but can significantly reduce the likelihood of cracking in the oxide. Both the crack length and the aspect ratio are fixed. As the spacing between the metal lines increases, the energy release rate decreases. When the aluminum lines are widely spaced, much of the oxide film is under compression, except in regions near the line, and the energy release rate drops to zero. Fig. 6(d) plots the energy release rate as a function of spacing for a crack located near the interface of the aluminum line. The energy release rate decreases slightly with increasing spacing but quickly plateaus

5. Channel crack

For a thin film of a brittle material supported by a tougher material, a crack can channel in the brittle film (Hutchinson and Suo, 1991) (Fig. 7). Here we explore the effect of constrained plasticity in the aluminum on a channel crack in the oxide. For the time being, assume all materials in the integrated structure are either linearly or nonlinearly elastic. When the length of the channel, L, exceeds a few times the thickness of the brittle film, t, the energy release rate at the channel front is independent of the length of the channel. Both the front of the channel and the opening of the wake of the channel maintain their shapes as the channel advances. Compare the elastic energy stored in a body without the channel and in a body with a long channel. Let y be the coordinate normal to the interface. At a temperature T, let $\delta(T, y)$ be the opening displacement in the body with the channel, and $\sigma(T, y)$ be the stress in the body without

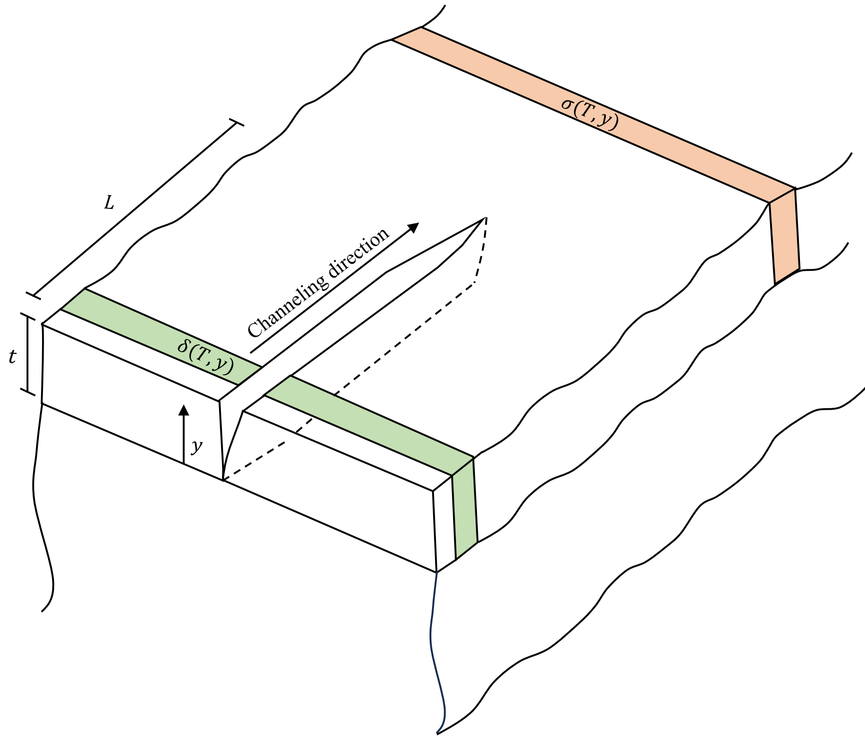

Fig. 7. Channel crack. For a channel crack to advance a unit distance, the reduction in the elastic energy is calculated from the elastic energy stored in a slice of material of unit thickness ahead of the crack front minus the elastic energy stored in a slice of material of unit thickness behind the crack front.

the channel. If $\sigma(T, y)$ is applied as the traction on the faces of the channel, the channel will be fully closed. After each temperature increment dT, the channel incrementally opens by displacement $d\delta = \delta(T + dT, y) - \delta(T, y)$. Associated with this incremental opening, the elastic energy in the body reduces by $L\sigma(T, y)d\delta dy$. Consequently, the elastic energy in the body with the channel is lower than the elastic energy in the body without the channel by the following amount:

$$U = L\int_0^t \int_0^\delta \sigma(T, y)d\delta dy \tag{3}$$

The energy release rate at the front of the channel is the reduction in the elastic energy in the body divided by the area of the channel:

$$G = \frac{U}{Lt} \tag{4}$$

A combination of the two previous equations gives the energy release rate at the front of the channel:

$$G = \frac{1}{t}\int_0^t \int_0^\delta \sigma(T, y)d\delta dy \tag{5}$$

An equation similar to Eq. (6) appeared in Beuth and Klingbeil (1996) for a film of uniform stress. Here we have generalized the expression for films of nonuniform stress. When all the materials in the integrated structure are linearly elastic, Eq. (6) reduces to (Hutchinson and Suo, 1991).

$$G = \frac{1}{2t}\int_0^t \sigma(T, y)\delta(T, y)dy \tag{6}$$

For a partially filmed crack ($c/t < 1$). The energy release rate at the front of the crack is given by:

$$G = \frac{1}{c}\int_0^c \int_0^\delta \sigma(T, y)d\delta dy \tag{7}$$

To compute the energy release rate at the front of a long channel, we need the solutions of two boundary value problems under plane-strain conditions. A boundary value problem without a channel is solved to determine the stress $\sigma(T, y)$ and a boundary value problem with a channel is solved to determine the crack opening displacement $\delta(T, y)$. Both boundary value problems are solved incrementally using ABAQUS to determine the stress and displacement as a function of temperature. Incidentally, for the integrated structure studied in this paper, the aluminum line may undergo plastic deformation. Consequently, as the channel advances, the aluminum line may undergo unloading. The loading and unloading of an elastic-plastic material undergo hysteresis, which affects the energy release rate at the channel front. This effect of hysteresis is unaccounted for in the above description, which assumes all materials in the integrated structure are elastic. To simplify the problem, we focus on the situation in which a long channel preexists, and we determine the condition for the channel to start to grow, such that no unloading occurs. Under proportional loading of multiaxial stresses, the plastic deformation of the metal is indistinguishable from that of a nonlinear elastic material. For an integrated structure, as temperature changes, the multiaxial stresses in the aluminum line are not strictly proportional loading. Here, to simplify the analysis, we will still ignore the effect of non-proportional loading, and model the elastic-plastic deformation of aluminum as nonlinear elastic deformation.

We now study the energy release rate at a long channel in the middle of the oxide layer. First, consider a long channel in the middle of the oxide between two aluminum lines. In the wake of the channel, the opening displacement is the same as that of a plane-strain crack of width c. Fig. 8(a) plots the normalized energy release rate at the channel front versus c for different values of the yield strength. Similar to the 2D edge crack, a lower yield strength results in a lower energy release rate. However, the energy release rate at the channel front does not drop to zero as the crack approaches the silicon nitride interface. We use the critical flaw size $c/t = 1$ to plot the energy release rate at the channel front as a function of aspect ratio (Fig. 8b). The behavior is similar to that of the edge crack. Thus, the same design conclusions apply for both edge cracks and channel cracks. Note that the energy release rate at the channel front is generally lower than that of the edge crack. Similar calculations are done for a long channel at the corner of the oxide, near the aluminum line (Fig. 8c,d).

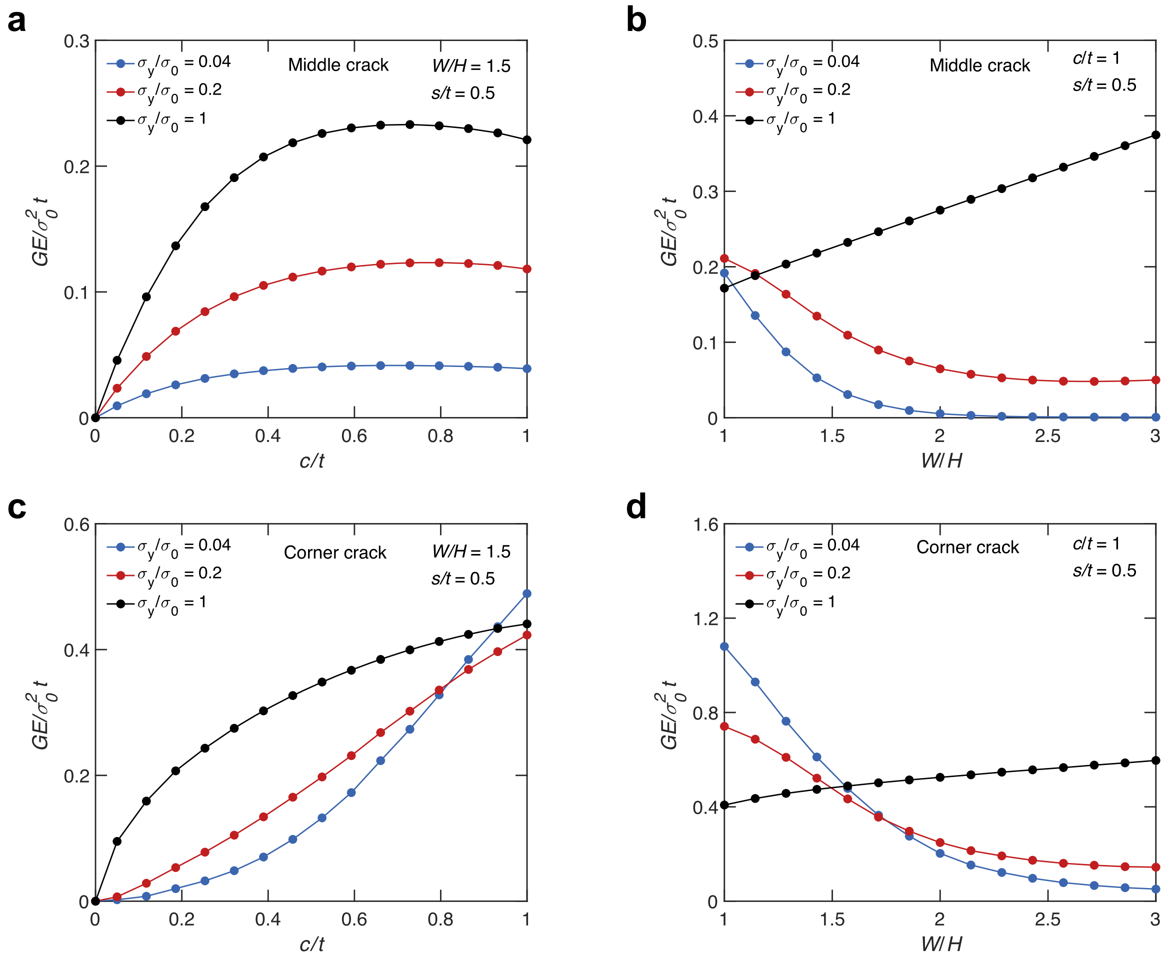

Fig. 8. Energy release rate at the channel front (a) Energy release rate at the channel front in the middle of the oxide as a function of c. (b) Energy release rate at the channel front in the middle of the oxide as a function of aspect ratio. (c) Energy release rate at the channel front near the aluminum interface as a function of c. (d) Energy release rate at the channel front near the aluminum interface as a function of aspect ratio.

6. Concluding remarks

We have studied an integrated structure in which a metal line is encased by a silicon substrate and a brittle oxide layer. In the triaxially constrained metal, the stresses readily exceed the yield strength of the metal, which can elevate the stresses in the oxide. We vary the degree of constraint in the metal by varying the aspect ratio of the metal. We have shown that the stresses in the oxide are sensitive to the geometry of the metal. Our results also indicate the energy release rate of edge cracks and long channels in the oxide are dependent on the geometry of the metal. In particular, an increase in the aspect ratio of the metal relieves the hydrostatic stresses and allows more plastic deformation to occur. However, the trends of the energy release rate associated with the amount of plastic deformation depend on the location of the crack. For cracks located in the midpoint between the two aluminum lines, an increase in the amount of plastic flow tends to relieve stresses and therefore decrease the energy release rate. For cracks located near the aluminum interface, plasticity simultaneously relieves stresses and increases the crack opening displacement of cracks. Because metal lines in semiconductor devices are commonly triaxially constrained, our analysis has implications for the design of these structures.

Statement of novelty

To the best of our knowledge, no existing work has a significant overlap with our submission.

CRediT authorship contribution statement

Sammy Hassan: Writing – review & editing, Writing – original draft, Software, Methodology, Investigation, Formal analysis, Conceptualization. **Jyun-Lin Wu:** Resources, Project administration. **Jason Lan:** Resources, Project administration. **Sherwin Tang:** Resources, Project administration. **Jun He:** Resources, Project administration, Funding acquisition. **Joost J. Vlassak:** Writing – review & editing. **Zhigang Suo:** Writing – review & editing, Supervision, Methodology, Funding acquisition.

Declaration of competing interest

The authors declare no conflict of interest.

Data availability

Data will be made available on request.

Acknowledgments

The work at Harvard was supported by a contract from TSMC.

References

Ang, D., Wong, C.C., Ramanujan, R.V., 2007. The effect of aspect ratio scaling on hydrostatic stress in passivated interconnects. Thin Solid Films 515, 3246–3252. https://doi.org/10.1016/j.tsf.2006.01.053.

Beuth, J.L., Klingbeil, N.W., 1996. Cracking of thin films bonded to elastic-plastic substrates. J. Mech. Phys. Solids 44, 1411–1428. https://doi.org/10.1016/0022-5096(96)00042-7.

Bromley, E.I., Randall, J.N., Flanders, D.C., Mountain, R.W., 1983. A technique for the determination of stress in thin films. J. Vac. Sci. Technol. B Microelectron. Process. Phenom. 1, 1364–1366. https://doi.org/10.1116/1.582744.

Chen, C.-P., Chen, Y., Subbarayan, G., Lin, H.-Y., Gurrum, S., n.d. A mechanistic model for plastic metal line ratcheting induced BEOL cracks in molded packages. 2022.

Cheng, E.J., Shen, Y.-L., 2012. Thermal expansion behavior of through-silicon-via structures in three-dimensional microelectronic packaging. Microelectron. Reliab. 52, 534–540. https://doi.org/10.1016/j.microrel.2011.11.001.

Flinn, P.A., Mack, A.S., Besser, P.R., Marieb, T.N., 1993. Stress-induced void formation in metal lines. MRS Bull. 18, 26–35. https://doi.org/10.1557/S0883769400039051.

Gouldstone, A., Shen, Y.-L., Suresh, S., Thompson, C.V., 1998. Evolution of stresses in passivated and unpassivated metal interconnects. J. Mater. Res. 13, 1956–1966. https://doi.org/10.1557/JMR.1998.0275.

Hutchinson, J.W., Suo, Z., 1991. Mixed mode cracking in layered materials. Advances in Applied Mechanics. Elsevier, pp. 63–191. https://doi.org/10.1016/S0065-2156(08)70164-9.

Jawarani, D., Kawasaki, H., Yeo, I.-S., Rabenberg, L., Stark, J.P., Ho, P.S., 1997. *In situ* transmission electron microscopy study of plastic deformation in passivated Al–Cu thin films. J. Appl. Phys. 82, 171–181. https://doi.org/10.1063/1.365584.

Jiang, T., Im, J., Huang, R., Ho, P.S., 2015. Through-silicon via stress characteristics and reliability impact on 3D integrated circuits. MRS Bull. 40, 248–256. https://doi.org/10.1557/mrs.2015.30.

Lee, J., Ma, Q., Marieb, T., Mack, A.S., Fujimoto, H., Flinn, P., Woolery, B., Keys, L., 1995. Measurement and modeling of intrinsic stresses in CVD W lines. MRS Proc. 391, 115. https://doi.org/10.1557/PROC-391-115.

Liu, X.H., Suo, Z., Ma, Q., Fujimoto, H., 2000. Developing design rules to avert cracking and debonding in integrated circuit structures. Eng. Fract. Mech. 66, 387–402. https://doi.org/10.1016/S0013-7944(00)00024-2.

Park, Y.-B., Jeon, I.-S., 2003. Mechanical stress evolution in metal interconnects for various line aspect ratios and passivation dielectrics. Microelectron. Eng. 69, 26–36. https://doi.org/10.1016/S0167-9317(03)00226-0.

Sautera, A.I., Nix, W.D., 1990. Finite element calculations of thermal stresses in passivated and unpassivated lines bonded to substrates. MRS Proc. 188, 15. https://doi.org/10.1557/PROC-188-15.

Shen, Y.-L., 2008. Externally constrained plastic flow in miniaturized metallic structures: a continuum-based approach to thin films, lines, and joints. Prog. Mater. Sci. 53, 838–891. https://doi.org/10.1016/j.pmatsci.2008.03.001.
Shen, Y.-L., 1997. Modeling of thermal stresses in metal interconnects: effects of line aspect ratio. J. Appl. Phys. 82, 1578–1581. https://doi.org/10.1063/1.365944.
Sullivan, T.D., 1996. Stress-induced voiding in microelectronic metallization: void growth models and refinements. Annu. Rev. Mater. Sci. 26, 333–364. https://doi.org/10.1146/annurev.ms.26.080196.002001.